Series resistance influence on performance of waveguide-type germanium photodetectors on silicon

Jeong-Min Lee (李楨敏), Minkyu Kim (金玟圭), and Woo-Young Choi (崔佑榮)*

Department of Electrical and Electronic Engineering, Yonsei University, Seoul 120-749, South Korea
*Corresponding author: wchoi@yonsei.ac.kr

We investigate influences of series resistances on the performance of 1.55 μm waveguide-type germanium photodetectors (Ge-PDs) on a silicon-on-insulator substrate. The current–voltage characteristics, responsivities, saturation photo-current characteristics, electrical reflection coefficients, and photodetection frequency responses of Ge-PDs, having different series resistances, are measured, and their equivalent circuit models are established. By analyzing the resulting circuit model parameters, we determine how much Ge-PD series resistances influence Ge-PD saturation photo-currents and photodetection bandwidth. These results should be of great use for optimization of Ge-PD fabrication processes and device parameters for target applications.

OCIS codes: 040.5160, 040.6040, 060.0060, 060.4510.
doi: 10.3788/COL201715.100401.

Si photonics is attracting a great amount of research interests, as it can provide cost-effective photonic solutions for various applications, such as optical interconnects[1], high-performance computing[2], bio-medical sensors[3], and radio-over-fiber systems[4]. One of the key components for Si photonic solutions in such applications are the 1.3–1.5 μm waveguide-type Ge-on-Si photodetector (Ge-PD), which can be realized along with other photonic components by the CMOS compatible Si processing technology. There have been several reports in which various device factors that influence Ge-PD performances have been investigated[5–7]. Influences of Ge layer thickness and length to the amount of the absorbed optical power, the junction capacitance[5], and photo-generated carrier transit time[6] have been investigated. The effect of electrode spacing on dark currents and the photodetection bandwidth has been also characterized[7].

In this Letter, our interest lies in determining influences of series resistances on Ge-PD performance. Although they are a parasitic effect, they can greatly influence Ge-PD photodetection bandwidth and saturation photo-currents. In optical interconnect applications, the Ge-PD bandwidth is of great importance. Radio-over-fiber systems require large saturation photo-currents for enhancing the dynamic range[4]. We design and fabricate two types of Ge-PDs, having different series resistances, and perform detailed measurements. From the measurement results, we establish equivalent circuit models for Ge-PDs and, using the extracted model parameters, we investigate how series resistances influence such Ge-PD performance parameters, such as saturation photo-currents and photodetection bandwidth.

Figures 1(a) and 1(b) show the top-view and the cross-section of Ge-PDs investigated in this Letter. Ge-PDs are fabricated on a 220 nm thick silicon-on-insulator having a 2 μm thick buried-oxide layer (BOX) through the Institute of Microelectronics (IME) foundry service[8]. Our

Ge-PDs are composed of a highly n-doped Ge (N^{++}-Ge) layer, a 0.5 μm thick intrinsic Ge layer, and a 0.22 μm thick p-doped Si (P^+-Si and P^{++}-Si) layer. The device is nominally 7 μm wide on the top, 8 μm wide at the bottom, and

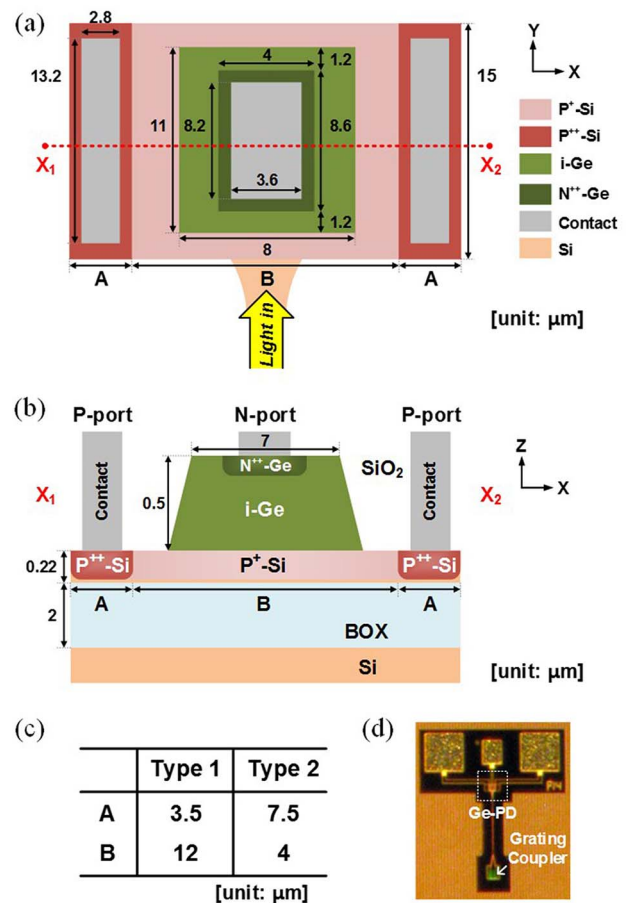Fig. 1. (a) Top-view, (b) cross-section, (c) design parameters, and (d) microphotograph of Type 1 Ge-PD.

11 μm long. The nominal peak doping concentrations are 1.27×10^{21} cm^{-3} for N^{++}-Ge, 3.5×10^{19} cm^{-3} for P^{+}-Si, and 5×10^{20} cm^{-3} for P^{++}-Si.

The series resistance (R_s) is composed of the contact resistance (R_c) and the resistance through p-doped Si layers (R_p) below the Ge absorption region. The fabrication process used for our Ge-PDs has no silicide step, resulting in relatively large contact resistance of 5500 $\Omega \cdot$ μm$^{2[9]}$. In order to reduce R_c as much as possible, our Ge-PDs have two parallel and relatively large (13.2 μm × 2.8 μm) contact openings, which provide about 75 Ω contact resistance. To investigate the influence of R_s on Ge-PD performance, two different types of devices are fabricated having different values for P^{+}-Si and P^{++}-Si region lengths, as shown in Fig. 1(c). Type 1 Ge-PD has a smaller P^{++}-Si region length resulting in larger R_s. Type 2 has a larger P^{++}-Si region length with the P^{+}-Si region narrower than the i-Ge region. Figure 1(d) shows the microphotograph of the fabricated Ge-PD (Type 1).

The influence of Ge-PD device parameters on the device performance can be identified by establishing Ge-PD equivalent circuit models and analyzing extracted model parameters[10,11]. A typical equivalent circuit model for p-i-n PD consists of a current source with the single-pole frequency response representing the photogenerated carrier transport[12,13]. Previously, we have shown that two current sources, one representing diffusing and the other drifting photogenerated carriers, provide more accurate modeling of the photogenerated carrier transport behavior within Ge-PDs[14]. Figure 2(a) shows such a two-current-source model, which is used for the present study. Here, I_1 and I_2 represent photogenerated carriers experiencing diffusion and drift, respectively. Figure 2(b) graphically shows frequency responses of I_1 and I_2 with time constant τ_1 for I_1 and τ_2 for I_2, along with the corresponding direct current (DC) gain A_1 and A_2, the sum of which represents Ge-PD DC responsivity normalized to one for simplicity.

Figure 2(a) also includes other circuit parameters that are needed for accurate modeling of Ge-PDs: C_j for the depletion capacitance, R_j for the drift region resistance, C_{c-c} for the capacitance between electrodes, C_{pad} for the pad capacitance, R_{int} for the interconnect resistance, and L_{int} for the interconnect inductance. For extracting numerical values of C_{pad}, R_{int}, and L_{int}, the measured reflection coefficients of open and short test patterns having the same geometry as the Ge-PD under investigation are used. The results are shown in Table 1. Numerical values for R_s, C_j, R_j, and C_{c-c} are obtained by comparing measured and simulated electrical reflection coefficients of Ge-PDs after the influence of C_{pad}, R_{int}, and L_{int} is de-embedded. Figures 3(a) and 3(b) show the resulting measured and simulated reflection coefficients on the Smith charts at two different bias voltages of −1 and −4 V. The figures show that, at each bias voltage, Type 1 and Type 2 Ge-PDs have the same imaginary part in their impedances, but Type 1 Ge-PD has a larger real part in the impedance than Type 2. This is because C_j's are the
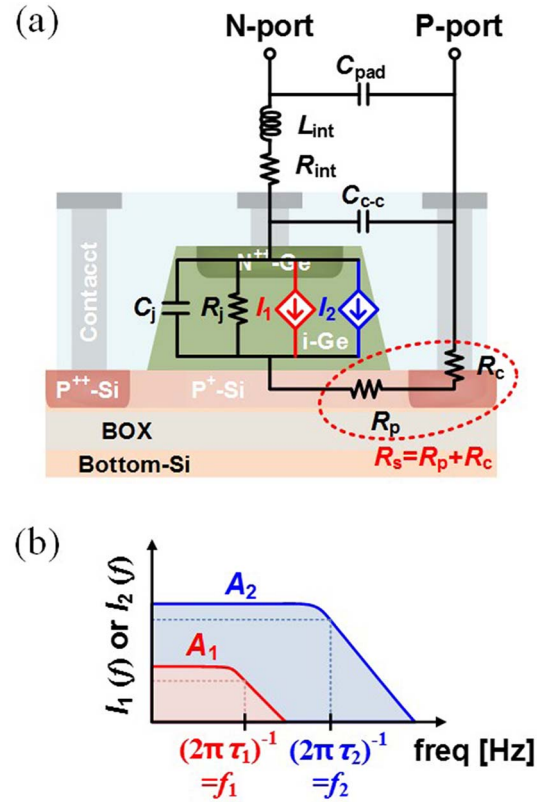

Fig. 2. (a) Modified equivalent circuit model of Ge-PD and (b) frequency responses of diffusing (I_1) and drifting (I_2) photogenerated carriers.

Table 1. Extracted Parameters for Pad and Interconnect

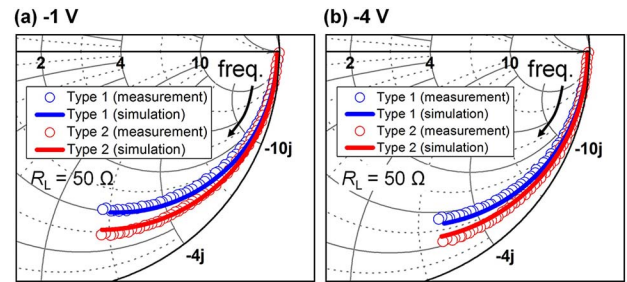| C_{pad} (fF)	R_{int} (Ω)	L_{int} (pH)
6.1	1.1	65

Fig. 3. (Color online) Measured and simulated reflection coefficients for Type 1 and 2 Ge-PDs from 100 MHz to 40 GHz at (a) −1 and (b) −4 V. Hollow circles represent the measurement results and solid lines as the simulation results.

same, but Type 1 has larger R_s. In addition, the larger reverse bias voltage results in the larger imaginary part of the impedance, since C_j is smaller. The extracted numerical values for R_s, C_j, R_j, and C_{c-c} are shown in Table 2. In particular, R_s for Type 1 and Type 2 Ge-PDs are 140 and

Table 2. Extracted Parameters for Ge P-I-N Junction

	Type 1		Type 2	
	−1 V	−4 V	−1 V	−4 V
R_s (Ω) $(=R_p + R_c)$	140 (=65 + 75)		88 (=13 + 75)	
C_j (fF)	15.9	11.6	15.9	11.6
R_j (kΩ)		20		
$C_{\text{c-c}}$ (fF)		6		
τ_1 (ps)	43	23.4	43	23.4
A_1 (%)	12.7	6.2	12.7	6.2
τ_2 (ps)		3.12		
A_2 (%)	87.3	93.8	87.3	93.8

88 Ω, respectively. R_s for different reverse biases has the same value because, although the depletion width changes with the bias voltage, this does not influence R_p, which is dominated by the resistance in the P^+-Si layer. C_j for both types are 15.9 and 11.6 fF at −1 and −4 V, respectively.

Numerical values for photo-current source parameters $(\tau_1, \tau_2, A_1, A_2)$ are obtained by technology computer-aided design (TCAD) simulated photodetection frequency responses for diffusing and drifting photogenerated carriers using the technique described in Ref. [14]. The resulting extracted values are listed in Table 2. As can be seen, the parameter values for both Ge-PDs are almost the same since R_s does not significantly affect the profiles of the electric field and photo-generated carriers within the Ge-PD. A_1 becomes smaller at a higher reverse bias since, with the larger electric field, less photo-generated carriers diffusively transport.

For saturation photo-current characterization, photo-currents for different incident optical powers at several different bias voltages are measured. For these measurements, 1.55 μm light is injected into the device through an on-chip grating coupler. The desired optical power is provided with an Er-doped fiber amplifier and a variable optical attenuator. A polarization controller is used so that only TE-polarized light is coupled into the Ge-PD.

Figures 4(a) and 4(b) show measured photo-currents of Type 1 and Type 2 Ge-PDs for different incident optical powers at two different bias voltages, respectively. At the small input optical power less than 1 mW, both Ge-PDs have almost constant responsivities of about 0.45 A/W. However, at large input optical powers, photo-currents saturate due to the space charge effect in both types of devices[15]. Saturation photo-currents ($I_{\text{ph,sat}}$) are substantially less for the Type 2 Ge-PD. This is because photo-currents flow through R_s and, in the Type 2 Ge-PD with smaller R_s, they experience a smaller voltage drop in the p-doped Si region, which results in the larger electric fields in the depletion region and suffers less from the space charge effect than Type 1. $I_{\text{ph,sat}}$ can be estimated as
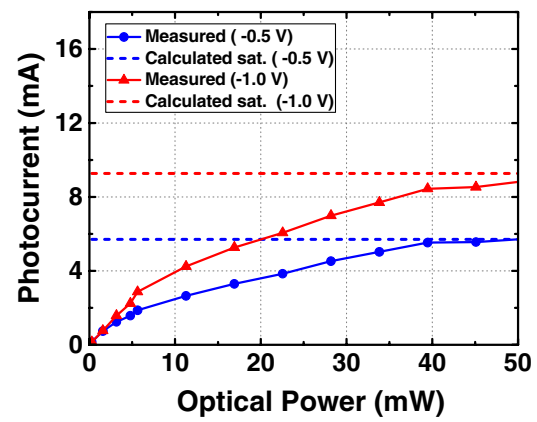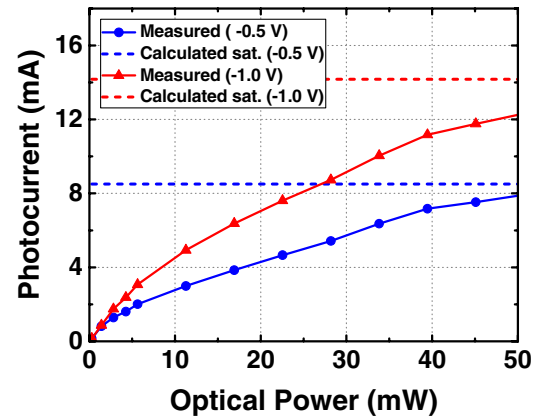
(a) Type 1

(b) Type 2

Fig. 4. (Color online) Measured photo-current versus input optical power at different bias voltages and calculated saturation photo-currents for (a) Type 1 and (b) Type 2 Ge-PDs $(R_L = 0.2\ \Omega)$.

$(V_{\text{Bias}} + V_{\text{bi}})/(R_s + R_L)$, where V_{bi} represents the built-in potential inside the Ge-PD, having a value of about 0.65 V, and R_L the load resistance of the measurement equipment having a value of 0.2 Ω. The estimated values are shown as dotted lines in Fig. 4. Figure 5 shows
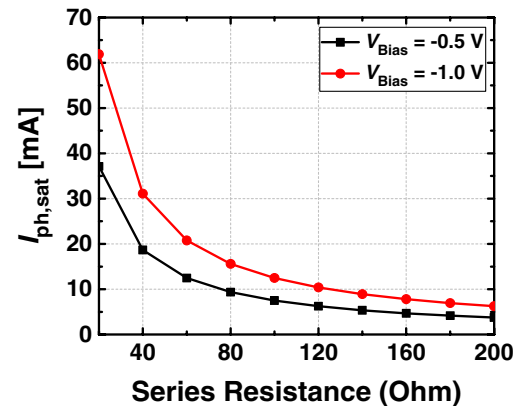

Fig. 5. (Color online) Influence of Ge-PD series resistance to saturation photo-currents at different bias voltages $(R_L = 0.2\ \Omega)$.

estimated $I_{\mathrm{ph,sat}}$'s for different R_s's at two different bias voltages of -0.5 and -1 V. As can be seen in this figure, Ge-PDs having smaller R_s have larger $I_{\mathrm{ph,sat}}$.

To characterize effects of R_s on photodetection frequency responses, two types of Ge-PDs are measured with a lightwave component analyzer from 100 MHz to 40 GHz with 160 µW optical power into Ge-PDs biased at -1 and -4 V. Figure 6 shows the measured photodetection frequency responses as well as simulated results. Simulations are done with the parameter values given in Table 2. As can be seen in Fig. 6, Ge-PDs have larger photodetection bandwidth at a larger reverse bias voltage due to the smaller junction capacitance that results in the smaller RC time constant. In addition, the Type 2 Ge-PD has the larger photodetection bandwidth than Type 1 due to smaller R_s that results in the smaller RC time constant.

Figures 7(a) and 7(b) show simulated photodetection bandwidths at -1 and -4 V for various values of R_s, respectively. Simulation results in Fig. 7 are obtained by using an equivalent circuit model in Fig. 2 for three cases: one including all three time constants of τ_1, τ_2, and τ_{RC} (RC time constant due to C_j, R_s, and R_L), second only τ_{RC}, and third including only τ_1 and τ_2. As can be seen in the figure, the photodetection bandwidth is mostly limited by carrier transport for our Ge-PDs. However, different τ_{RC} values due to different bias voltages and/or R_s also influence the photodetection bandwidth. From these, it is clear that we have to first reduce the photogenerated carrier transit time in our Ge-PDs and, furthermore, reduce R_s in order to realize Ge-PDs having the highest possible photodetection bandwidth. The

Fig. 7. (Color online) Influence of series resistance to photodetection bandwidth according to three different time constants of τ_1, τ_2, and τ_{RC} at (a) -1 and (b) -4 V ($R_L = 50\ \Omega$).
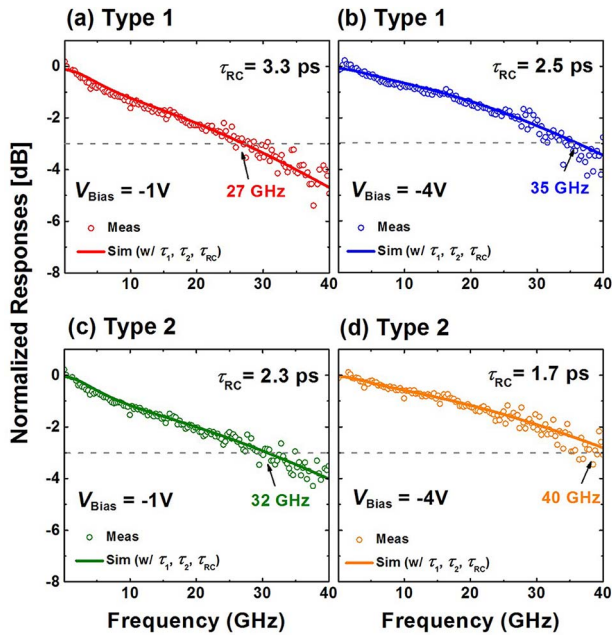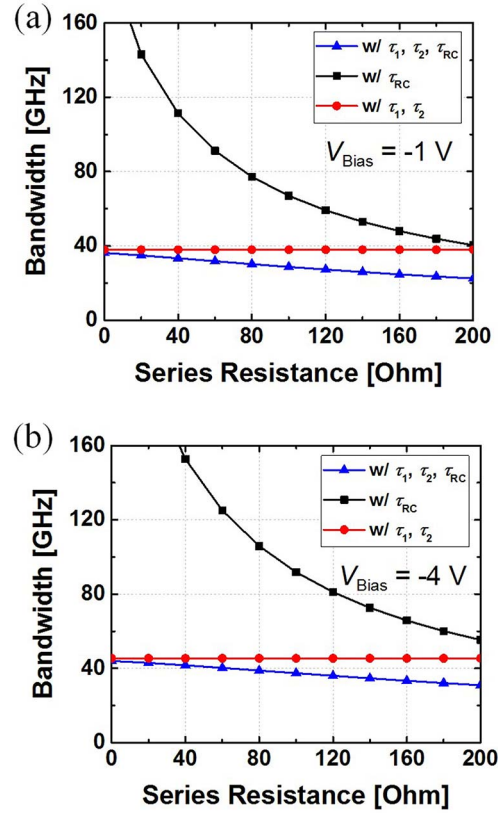

Fig. 6. Measured and simulated photodetection frequency responses from 100 MHz to 40 GHz for Type 1 Ge-PD at (a) -1 and (b) -4 V and Type 2 Ge-PD at (c) -1 and (d) -4 V at 160 µW input optical power to Ge-PDs ($R_L = 50\ \Omega$).

quantitative determination of key device parameters clearly helps the identification of the parameters that limit Ge-PD performance and finding out the directions for performance improvement.

We investigate the influence of series resistances on current–voltage characteristics, saturation photo-current characteristics, and photodetection bandwidths for two types of Ge-PDs having different series resistances. Accurate equivalent circuit models are developed, which provide well-matching simulation results with measurement results of Ge-PDs. With these models, we are able to determine accurate quantitative values for key Ge-PD parameters. We demonstrate that Ge-PD series resistances have a strong influence on photodetection saturation characteristics and photodetection frequency responses. Our equivalent circuit model, as well as the procedure we used for exacting model parameter values, should be very useful for optimizing the Ge-PD device structure.

References

1. R. Soref, IEEE J. Sel. Top. Quantum Electron. **12**, 1678 (2006).
2. C. Sun, M. T. Wade, Y. Lee, J. S. Orcutt, L. Alloatti, M. S. Georgas, A. S. Waterman, J. M. Shainline, R. R. Avizienis, S. Lin, B. R. Moss, R. Kumar, F. Pavanello, A. H. Atabaki, H. M. Cook, A. J. Ou, J. C. Leu, Y.-H. Chen, K. Asanović, R. J. Ram, M. A. Popović, and V. M. Stojanović, Nature **528**, 534 (2015).
3. K. Zinoviev, L. G. Carrascosa, J. S. d. Río, B. Sepúlveda, C. Domínguez, and L. M. Lechuga, Adv. Opt. Technol. **2008**, 1 (2008).
4. B. Pal, *Frontiers in Guided Wave Optics and Optoelectronics* (InTech, 2010).
5. M. Rouvière, M. Halbwax, J.-L. Cercus, E. Cassan, L. Vivien, D. Pascal, M. Heitzmann, J.-M. Hartmann, and S. Laval, Opt. Eng. **44**, 075402-1 (2005).
6. K. Kato, IEEE Trans. Microwave Theory Tech. **47**, 1265 (1999).
7. M. Rouvière, L. Vivien, X. Le Roux, J. Mangeney, P. Crozat, C. Hoarau, E. Cassan, D. Pascal, S. Laval, J.-M. Fédéli, J.-F. Damlencourt, J. M. Hartmann, and S. Kolev, Appl. Phys. Lett. **87**, 231109 (2005).
8. A. Novack, Y. Liu, R. Ding, M. Gould, T. Baehr-Jones, Q. Li, Y. Yang, Y. Ma, Y. Zhang, K. Padmaraju, K. Bergmen, A. E.-J. Lim, G.-Q. Lo, and M. Hochberg, in *Proceedings of Group IV Photonics* (2013).
9. T. Pinquet, *IME OpSIS Design Rule Manual*, OpSIS, Rev 1.5 (2012).
10. M.-J. Lee and W.-Y. Choi, IEEE Trans. Electron Devices **60**, 998 (2013).
11. M.-J. Lee, H.-S. Kang, and W.-Y. Choi, IEEE Electron Device Lett. **29**, 1115 (2008).
12. M. Piels, A. Ramaswamy, and J. E. Bowers, Opt. Express **21**, 15634 (2013).
13. M. Gould, T. Baehr-Jones, R. Ding, and M. Hochberg, Opt. Express **20**, 7101 (2012).
14. J.-M. Lee, S.-H. Cho, and W.-Y. Choi, IEEE Photon. Technol. Lett. **28**, 2435 (2016).
15. S. M. Sze and K. K. Ng, *Physics of Semiconductor Devices* (Wiley, 2007).